

Swarming dynamics under different orientation (chiral) coupling mechanisms

A. Author,¹ ^{a)} B. Author,¹ and C. Author², ^{b)}

¹⁾Authors' institution and/or address

²⁾Second institution and/or address

(*Electronic mail: Second.Author@institution.edu.)

(Dated: 31 March 2024)

An article usually includes an abstract, a concise summary of the work covered at length in the main body of the article. It is used for secondary publications and for information retrieval purposes.

I. INTRODUCTION

Synchronization and swarming are two typical self-organization behaviors representing the intrinsic dynamical and spatial ordering of units in complex systems. The study of self-organized coordination of intrinsic degrees of freedom/rhythms within complex systems has deepened our understanding of self-organization in complex systems, including various levels of synchronization, partial synchronization, extended states, and chimera states^{1–6}. In terms of synchronization theory, at the micro level, various analysis methods have been established, such as the master stability function (MSF)⁷, which has played an important role in the study of multi-oscillator synchronization problems. At the statistical and macro levels, successful approaches include the self-consistent equation method by Kuramoto et al.⁸, the Watanabe-Strogatz transformation^{9,10}, and the Ott-Antonsen ansatz proposed by Ott and Antonsen¹¹. Cluster behavior research focuses on the self-organized coordination of spatial movement in complex systems, contributing to our understanding of collective behavior. Spatial cluster behavior can emerge at different scales, such as animal clusters^{12,13}, bacterial directed motion^{14,15}, and other phenomena^{16–18}. Numerous studies based on diverse cluster models and extensive experimental investigations^{19–25} have revealed various collective spatial interactions and patterns in complex systems.

The Kuramoto model and the Vicsek model are two well-known models that describe synchronization and swarming, respectively. The Kuramoto model describes the synchronization of oscillators with a phase variable, and the Vicsek model describes the alignment of self-propelled particles with a velocity variable. Both models have been widely studied and applied in various fields, such as physics^{26,27}, biology^{28–31}, and engineering^[32,33,37].

II. MODEL

Oscillators have a spatial position $\mathbf{r}_i = (x_i, y_i)$ and an internal phase θ_i which evolve according to equations:

$$\dot{x}_i = v \cos \theta_i , \quad (1)$$

$$\dot{y}_i = v \sin \theta_i , \quad (2)$$

$$\dot{\theta}_i = \omega_i + \lambda \sum_{j=1}^N A_{ij} \sin(\theta_j - \theta_i) \quad (3)$$

for $i = 1, 2, \dots, N$, where N is the number of oscillators. As per Eq. (1) and (2), each oscillator moves with a constant speed v in the direction of its current phase θ_i . The phase θ_i evolves according to Eq. (3), where ω_i is the natural frequency of the i th oscillator, λ is the coupling strength, and A is the adjacency matrix of the network, with $A_{ij} = 1$ if there is a connection from i th to j th oscillator, and $A_{ij} = 0$ otherwise. We can consider Eq. (1)–(3) as a generalization of the Kuramoto model and the Vicsek model in the sense that it includes both the phase and the spatial position of the oscillators.

Each oscillator i is connected to all the oscillators within a action radius d_0 of its position. The adjacency matrix A is defined as:

$$A_{ij} = \begin{cases} 1, & |\mathbf{r}_i - \mathbf{r}_j| \leq d_0 \\ 0, & |\mathbf{r}_i - \mathbf{r}_j| > d_0 \end{cases} \quad (4)$$

where $|\mathbf{r}_i - \mathbf{r}_j|$ is the Euclidean distance between the i th and j th oscillators.

For simplicity, we consider oscillators are initially distributed uniformly in a two-dimensional square with side length L and periodic boundary conditions. Their positions $\mathbf{r}_i(t) = (x_i(t), y_i(t))$ at given time t are given by:

$$\begin{aligned} x_i(t + \Delta t) &= x_i(t) + v \cos \theta_i(t) \Delta t \bmod L, \\ x_i(t + \Delta t) &= x_i(t) + v \cos \theta_i(t) \Delta t \bmod L, \end{aligned} \quad (5)$$

where Δt is the discrete time step. When two oscillators are on opposite sides of the square, the absolute value of the difference between one of their coordinates is greater than $L/2$. In this case, we take the minimum distance between them, which is the distance between the two points in the periodic boundary conditions. For a given pair of points \mathbf{r}_i and \mathbf{r}_j , the distance between them is $|\mathbf{r}_i - \bar{\mathbf{r}}_j|$, where $\bar{\mathbf{r}}_j = (\bar{x}_j, \bar{y}_j)$ is the

^{a)}Also at Physics Department, XYZ University.

^{b)}<http://www.Second.institution.edu/~Charlie.Author>.

adjusted position of the j th oscillator, given by:

$$\bar{x}_j = \begin{cases} x_j, & |x_i - x_j| \leq L/2 \\ x_j + L, & x_i - x_j > L/2 \\ x_j - L, & x_j - x_i > L/2 \end{cases}, \quad (6)$$

$$\bar{y}_j = \begin{cases} y_j, & |y_i - y_j| \leq L/2 \\ y_j + L, & y_i - y_j > L/2 \\ y_j - L, & y_j - y_i > L/2 \end{cases}. \quad (7)$$

$|\mathbf{r}_i - \bar{\mathbf{r}}_j|$ can be proved to be the minimum distance between \mathbf{r}_i and \mathbf{r}_j in the periodic boundary conditions (see the proof in Appendix A).

Finally, we consider that the natural frequencies ω_i are distributed in two symmetric uniform distributions, representing two types of chirality. Exactly half of the oscillators have natural frequencies in the range $[\omega_{\min}, \omega_{\max}]$ ($\omega_i \sim U(\omega_{\min}, \omega_{\max}), i = 1, 2, \dots, N/2$) and the other half in the range $[-\omega_{\max}, -\omega_{\min}]$ ($\omega_i \sim U(-\omega_{\max}, -\omega_{\min}), i = N/2 + 1, N/2 + 2, \dots, N$).

III. BEHAVIOR

We performed numerical simulations of the model to probe the behavior of its solutions (see Appendix B for details on the numerical methods). $N = 1000$ oscillators were distributed uniformly in the square of length $L = 10$ and their natural frequencies were distributed in the range $[\omega_{\min}, \omega_{\max}] = [1, 3]$ and $[-\omega_{\max}, -\omega_{\min}] = [-3, -1]$. Two-parameter of coupling strength λ and action radius d_0 are presented in the phase diagram in Fig. 1. We found the system settles into five states: **Disorder**, **Ring**, **Swarm** (which can be further divided into **Multi-Clusters** and **Double-Clusters**), and **Quick Sync**. In Fig. 1 we show the snapshots of the last three states and where these states are located in the phase diagram. The Disorder state is shown in Fig. 2a. We next discuss these five states.

A. Disorder State

Disorder state occurs when both λ and d_0 are small. In this state, the oscillators are not asynchronous (phase histogram is uniform, like Fig. 3a) and move in a way which similar to uncoupled oscillators ($\lambda = 0$), as shown in Fig. 2a. According to Eq. (1)-(3), when $\lambda = 0$, the equations of oscillators' motion can be written as:

$$x_i(t) = x_i^0 + \frac{v}{\omega_i} \sin [\theta_i(0) + \omega_i t], \quad (8)$$

$$y_i(t) = y_i^0 - \frac{v}{\omega_i} \cos [\theta_i(0) + \omega_i t]. \quad (9)$$

Then we have

$$(x_i - x_i^0)^2 + (y_i - y_i^0)^2 = \left(\frac{v}{\omega_i} \right)^2. \quad (10)$$

In such a setup, oscillators move in a circular trajectory with radius v/ω_i and the phases θ_i increase linearly with time, as

show in Fig. 2b. To calculate the real-time rotational radius, we first estimate real-time centers $\mathbf{c}(t)$ of the circular trajectory with method in Fig. 4 and then solve the following linear equations:

$$\begin{aligned} \mathbf{c}_i(t_1) \cdot \mathbf{v}_i(t_1) &= \mathbf{x}_i(t_1) \cdot \mathbf{v}_i(t_1), \\ \mathbf{c}_i(t_2) \cdot \mathbf{v}_i(t_2) &= \mathbf{x}_i(t_2) \cdot \mathbf{v}_i(t_2), \end{aligned} \quad (11)$$

where $\mathbf{v}_i(t_1) = (x_i(t_1), y_i(t_1))$ is the velocity of i th oscillator at t_1 , and $\mathbf{v}_i(t_1) = (\cos \theta_i(t_1), \sin \theta_i(t_1))$ is the unit vector of the velocity. According to Eq. (1)-(3), we can calculate $\mathbf{v}_i(t_2)$ and $\mathbf{r}_i(t_2)$, ($t_2 = t_1 + \Delta t$).

The real-time rotational radius is $r_i(t) = |\mathbf{c}_i(t) - \mathbf{r}_i(t)|$. We found that the real-time rotational radius is almost constant and close to v/ω_i for each oscillator in the Disorder state, as shown in Fig. 5a. The estimation results of four states's real-time rotational centers are shown in Fig. 13 in Appendix.

B. Ring State

The Ring state is characterized by the oscillators forming several rings with thickness, each of which is composed of oscillators with the same chirality, as is show in Fig. 1a. Similar to Disorder state, the oscillators in the same ring cluster move in a circular trajectory with a constant rotational radius calculated in Fig. 5a. The oscillators' phase is uniformly distributed in the range $[-\pi, \pi]$ (cf. Fig. 3a), which leads to oscillators uniformly located on the circular trajectory. Fig. 6a shows there is a long transient time before this state is reached, and in this transient time, the trajectories of oscillators with the same chirality aggregate slowly. Conversely, the oscillators with different chirality repel each other.

C. Swarm State

Swarm State is a state where the oscillators form spatial clusters and align into several clusters [Fig. 1b, c and Fig. 6b]. When λ and d_0 increases, the number of clusters decreases by 2, which is named by Double-Clusters state, and other states are named by Multi-Clusters state. The clusters are composed of oscillators with the same chirality, and the phase θ_i of the oscillators in the same cluster is synchronized as seen in Fig. 3b and 3c, which means that the oscillators in the cluster move with the same velocity $\mathbf{v}_i = (\cos \theta_s, \sin \theta_s)$ and rotational radius $r_i = v/\theta_s$, where θ_s is the oscillators' phase in the cluster. Based on this property, we can calculate θ_s and r_i with Eq. (3):

$$\begin{aligned} N_s \omega_s &= \sum_{i=1}^{N_s} \left(\omega_i + \lambda \sum_{j=1}^{N_s} A_{ij} \sin (\theta_j - \theta_i) \right) \\ \omega_s &= \frac{1}{N_s} \sum_{i=1}^{N_s} \omega_i + \frac{\lambda}{N_s} \sum_{i=1}^{N_s} \sum_{j=1}^{N_s} A_{ij} \sin (\theta_j - \theta_i) \\ &= \frac{1}{N_s} \sum_{i=1}^{N_s} \omega_i, \end{aligned} \quad (12)$$

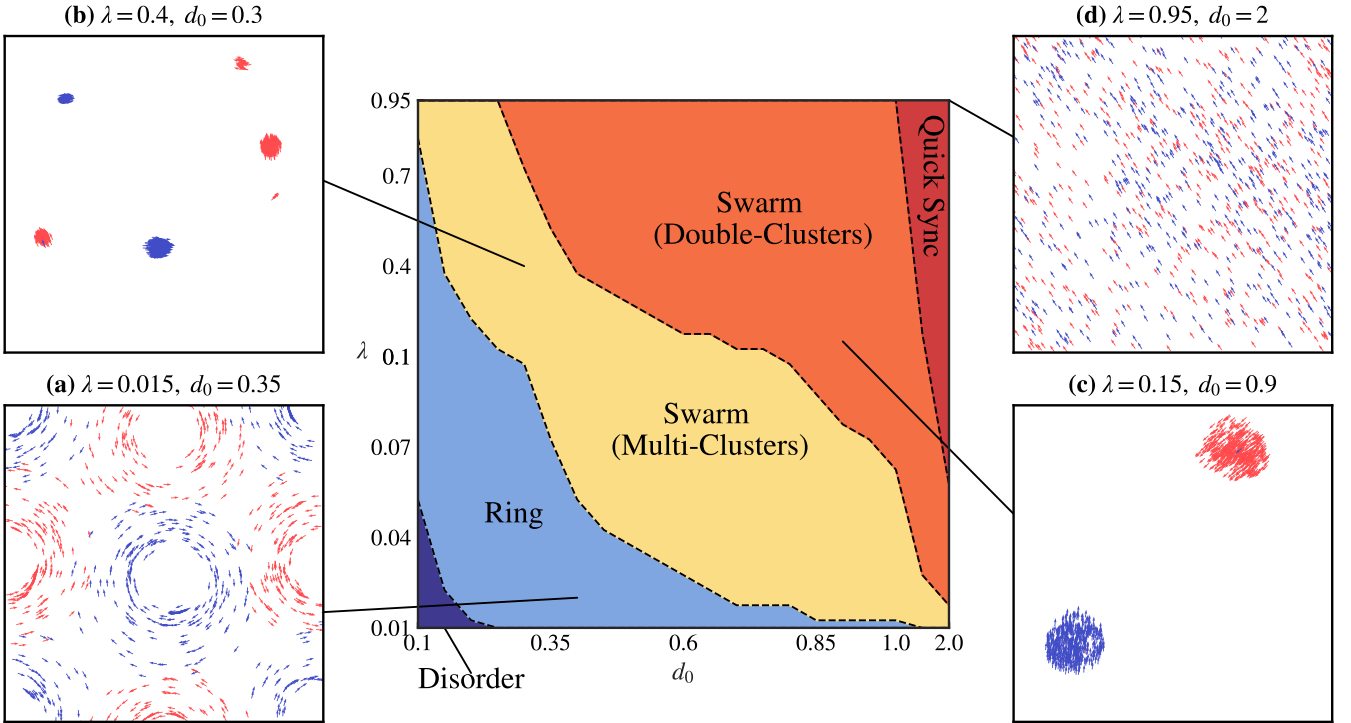


FIG. 1. Phase diagram of model Eq. (1)-(3) in the $(\lambda-d_0)$ plane. The boundaries between states are analytical approximations given by Subsection V A. For the sake of clarity, the scale of λ and d_0 is non-linear (For λ in $[0.01, 0.1]$ and $[0.1, 1]$, step length is 0.1 and 0.05, respectively. For d_0 in $[0.1, 1]$ and $[1, 2]$, step length is 0.05 and 0.5, respectively). (a), The snapshots of Ring ($\lambda = 0.015, d_0 = 0.35$). (b), Swarm (Multi-Clusters) ($\lambda = 0.4, d_0 = 0.3$). (c), Swarm (Double-Clusters) ($\lambda = 0.15, d_0 = 0.9$). (d), Quick Sync ($\lambda = 0.95, d_0 = 2$). Two types of chiral oscillators are represented by red ($\omega_i > 0$) and blue ($\omega_i < 0$) arrows, respectively.

where N_s is the number of oscillators in the cluster. As $\omega_i \sim U(\omega_{\min}, \omega_{\max})$ and $\omega_i \sim U(-\omega_{\max}, -\omega_{\min})$ for two types of chirality, we can calculate θ_i , ω_s and r_i with ω_i for Double-Clusters state:

$$\theta_i = \omega_s = \begin{cases} (\omega_{\max} + \omega_{\min})/2, & i = 1, 2, \dots, N/2 \\ -(\omega_{\max} + \omega_{\min})/2, & i = N/2 + 1, \dots, N \end{cases},$$

$$r_i = \frac{v}{|\omega_s|}, \quad (13)$$

as shown in Fig. 5b. But for Multi-Clusters, due to which oscillators are synchronized within each cluster is not accurately known, we can only calculate the real-time rotational radius of them. As seen in Fig. 5b, similar to Double-Clusters, some local platforms appear in the real-time rotational radius due to synchronization.

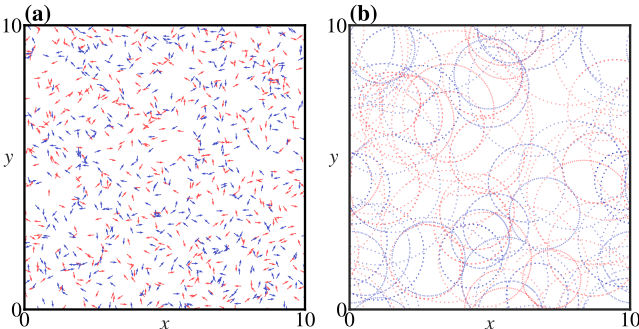


FIG. 2. Key properties of the Disorder state. (a), The snapshot of the Disorder state ($\lambda = 0.01, d_0 = 0.1, T = 60000$). (b), The scatter plot of last 100 time steps of 20 positive chirality oscillators and 20 negative chirality oscillators.

D. Quick Sync State

Quick Sync state is a simple state where total oscillators are synchronized quickly, as shown in Fig. 1d. and 3d. The oscillators are synchronized in an extremely short time, which leads them have no time to form clusters (can also be considered as a special case of Swarm state). Due to the two types of chirality oscillators are synchronized and the distributions of them is symmetric, the phase velocities of total oscillators are close to zero according to Eq. (12).

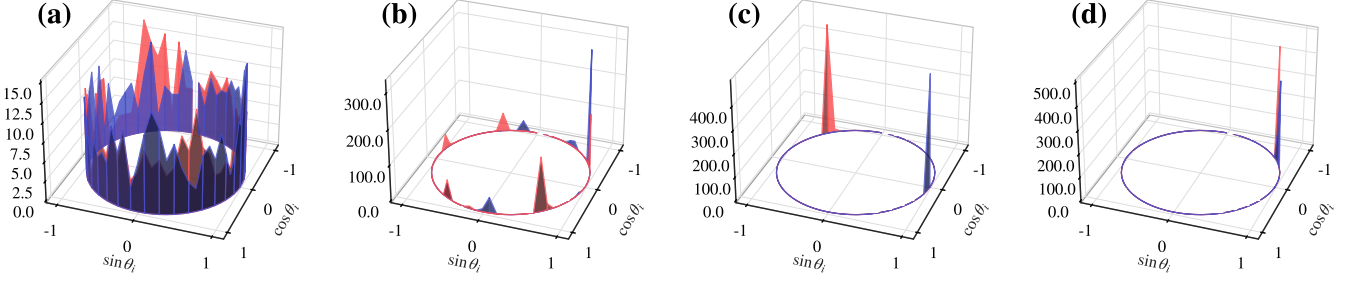


FIG. 3. Histogram of the oscillators' phases. (a), Ring state ($\lambda = 0.015$, $d_0 = 0.35$). (b), Swarm state (Multi-Clusters, $\lambda = 0.8$, $d_0 = 0.2$). (c), Swarm state (Double-Clusters, $\lambda = 0.15$, $d_0 = 0.9$). (d), Quick Sync state ($\lambda = 0.95$, $d_0 = 2$). The histograms are calculated with 70 bins.

IV. ORDER PARAMETER

Having described the four states of our system, we next discuss how to distinguish them. We use the order parameter R to measure global synchronization. The order parameter R is defined as:

$$R = \left| \frac{1}{N} \sum_{j=1}^N e^{i\theta_j} \right|. \quad (14)$$

The order parameter R is the absolute value of the mean of the complex numbers $e^{i\theta_i}$, which can be interpreted as the mean direction of the oscillators. When $R = 1$, the oscillators are completely synchronized, and when $R = 0$, the oscillators are completely desynchronized. Fig 7a shows the order parameter R in the parameter plane. The order parameter R is close to 1 in the Quick Sync state, close to 0 in the Disorder state and most of the Ring state, and between 0 and 1 in other states. In these states, we see that the order parameter R changes non-monotonically in the sense that phases in these states are not globally synchronized, and each cluster's phase velocity $\omega_s \neq 0$. When the phases of different clusters are exactly equal, the order parameter R is close to 1, and when they are exactly opposite, R is close to 0.

Having realized that the order parameter R is not enough to distinguish the states with clusters, we next define the following order parameter R_s to metric the local synchronization,

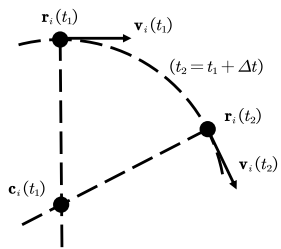


FIG. 4. Estimation for real-time centers. $c_i(t_j)$, $r_i(t_j)$ and $v_i(t_j)$ are the center of the circular trajectory, the position and the velocity of the i th oscillator at time t_j , respectively. The line from $c_i(t_j)$ to $r_i(t_j)$ is perpendicular to $v_i(t_j)$.

$$R_s = \frac{1}{N_c} \sum_{k=1}^{N_c} \left| \frac{1}{|C_k|} \sum_{j \in C_k} e^{i\theta_j} \right|, \quad (15)$$

where N_c is the number of clusters, C_k is the k th cluster, and $|C_k|$ is the number of oscillators in the k th cluster. We can consider R_s as an order parameter that studies the spatial position and internal phase simultaneously. To determine the classification of clusters, we use the following method: we first calculate the relative center distance matrix $D_{ij} = |\mathbf{c}_i - \bar{\mathbf{c}}_j|$, where $\bar{\mathbf{c}}_j = (\bar{x}_j, \bar{y}_j)$ is the adjusted position of the j th oscillator's rotational center calculated by Eq. (6), (7) and (11). The reason of using the distance between centers instead of the distance between oscillators' positions is that the oscillators in the Ring state are uniformly distributed on the circular trajectory, and the distance between them is much larger than the distance between their centers. Then we use the DBSCAN algorithm to cluster the oscillators. The DBSCAN algorithm is a density-based clustering algorithm, which can find clusters of arbitrary shapes and sizes. We set the minimum number of oscillators in a cluster to be 5 and the maximum distance between two oscillators in the same cluster to be 0.3 (see Appendix C for details on the determination of these parameters). One example of the classification of clusters is shown in Fig. 8. We then calculate the order parameter R_s for each cluster. The order parameter R_s is close to 1 in the Swarm state (R_s of Double-Clusters state is closer to 1 than Multi-Clusters) and Quick Sync state, and close to 0 in Disorder state and most of the Ring state, between 0 and 1 in other Ring states with local clusters, as shown in Fig. 7b.

Combining the order parameter R and R_s , we can find only the distinction between Ring and Disorder states has not been resolved. Except the study for synchronization, we also define an order parameter $\Delta\Omega$ to metric the phase locking of the oscillators:

$$\Delta\Omega = \frac{1}{N_c} \sum_{k=1}^{N_c} \left[\frac{1}{|C_k|^2} \sum_{i,j \in C_k} (\langle \dot{\theta}_i \rangle - \langle \dot{\theta}_j \rangle)^2 \right], \quad (16)$$

where $\langle \dot{\theta}_i \rangle$ is the average of the phase velocity of the i th clus-

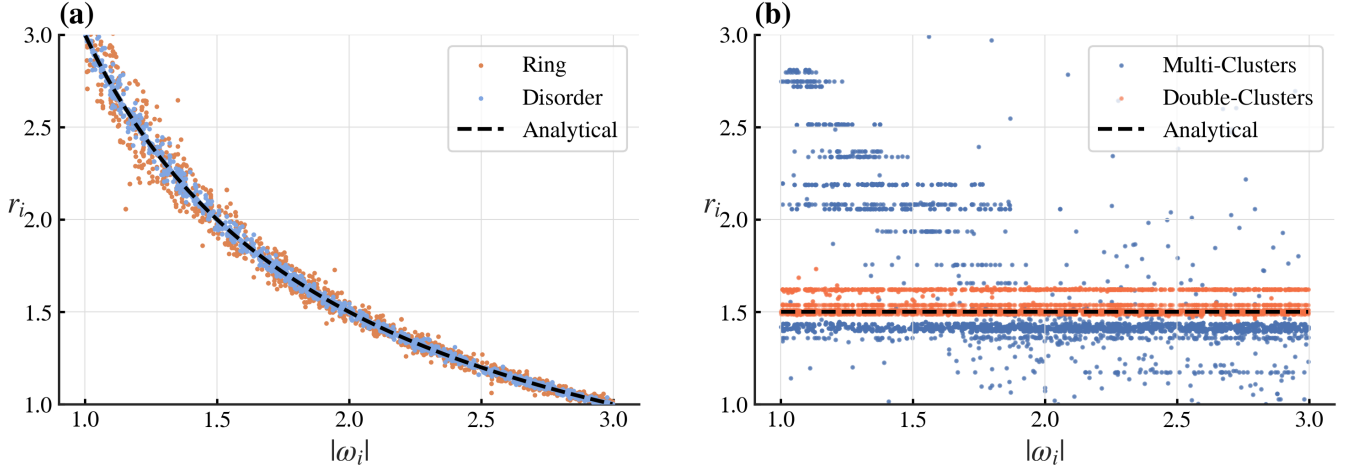


FIG. 5. The real-time and analytical rotational radius. (a), Radius for the Disorder ($d_0 = 0.1$, $\lambda = 0.01 : 0.06$) and Ring ($d_0 = 0.1$, $\lambda = 0.06 : 0.1$). The real-time rotational radius is almost constant and close to v/ω_i for each oscillator. (b), Radius for Swarm (Multi-Clusters, $d_0 = 0.15 : 0.25$, $\lambda = 0.95$) and (Double-Clusters, $d_0 = 2$, $\lambda = 0.02 : 0.05$). Analytical line is only for Double-Clusters. All the above simulations are calculated at $t = 60000$.

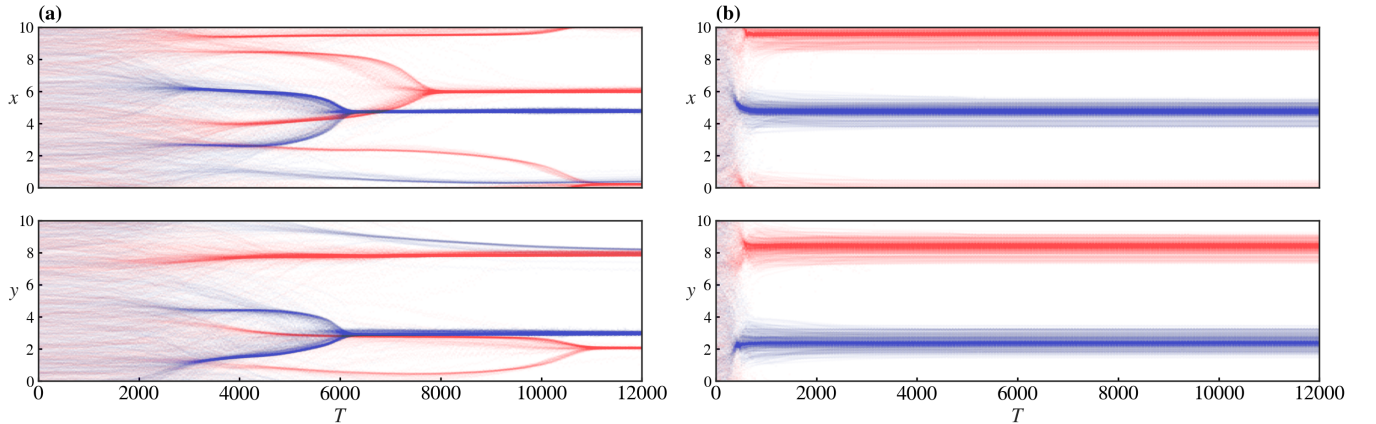


FIG. 6. Scatter plot of the real-time centers position. (a), centers position of Ring ($\lambda = 0.02$, $d_0 = 0.4$). As time goes on, the centers of oscillators with the same chirality converge. (b), centers position of Swarm ($\lambda = 0.01$, $d_0 = 2$). Unlike Ring, the centers converge quickly. The centers position are estimated with method in Fig. 4 and Eq. (11).

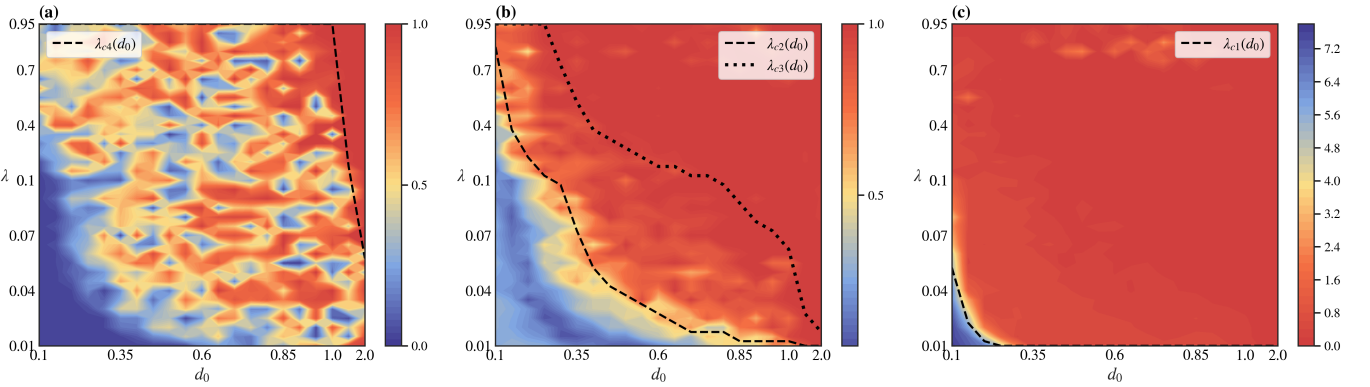


FIG. 7. Order parameter heatmaps of (λ, d_0) plane and the critical lines of the transitions between states. (a), order parameter R and critical line of $\lambda_{c4}(d_0)$. (b), order parameter R_s and critical lines of λ_{c2} , λ_{c3} . (c), order parameter $\Delta\Omega$ and critical lines of λ_{c1} . All order parameters are calculated at $t = 60000$.

TABLE I. Order parameter values in each state

State	R	R_s	$\Delta\Omega$
Disorder	$= 0$	$= 0$	> 0
Ring	$= 0$	$= 0$	$= 0$
Swarm (Multi-Clusters)	> 0	$\rightarrow 1^{\text{a}}$	$= 0$
Swarm (Double-Clusters)	> 0	$\approxeq 1^{\text{a}}$	$= 0$
Quick Sync	$= 1$	$= 1$	$= 0$

^a Note that the R_s of Double-Clusters state is closer to 1 than that of Multi-Clusters state.

ter, which can be calculated by

$$\langle \dot{\theta}_i \rangle = \lim_{T \rightarrow \infty} \frac{1}{T} \int_{t_0}^{t_0+T} \dot{\theta}_i(t) dt. \quad (17)$$

We estimate $\langle \dot{\theta}_i \rangle$ by the average of the phase velocity of the oscillators in the i th cluster at the last 1000 time steps. The order parameter $\Delta\Omega > 0$ in the Disorder state, and $\Delta\Omega = 0$ in other states, as shown in Fig. 7c.

To sum up, using R , R_s and $\Delta\Omega$ in combination allows us to discern all the equilibrium state of our system. The order parameter values in each state are summarized in Table I.

V. ANALYSIS

A. Analytical approximations of the critical boundaries

In this section we derive the analytical approximations of the boundaries between the states. The boundaries between the states are determined by the critical lines λ_{c1} , λ_{c2} , λ_{c3} , and λ_{c4} , which are the critical values of λ for the transitions between the states with given d_0 .

1. λ_{c1} : Disorder to Ring

We first consider the transition between the Disorder and Ring states. The oscillators in both states move in a circular trajectory (cf. Fig. 2b), and the difference between them is

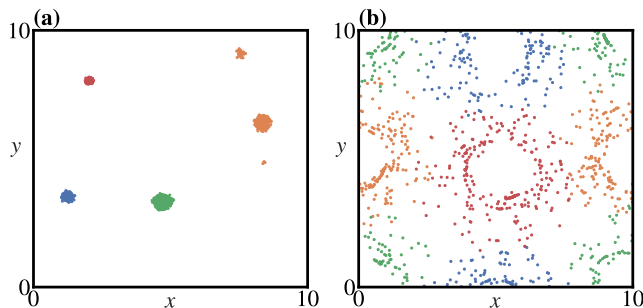


FIG. 8. Two examples of classification results. (a): ($\lambda = 0.4$, $d_0 = 0.3$). (b): ($\lambda = 0.02$, $d_0 = 0.4$).

that the oscillators in the Ring state are phase-locked. Therefore, oscillators in Disorder state have a very small probability of being randomly distributed on the ring, but without phase locking. The critical coupling strength λ_{c1} can be calculated as the critical value of λ for the phase locking of oscillators on the same ring. We consider the following synchronous dynamics of oscillators on the same ring:

$$\dot{\theta}_1 = \omega_1 + \lambda \sum_{j=2}^{N_c} A_{1j} \sin(\theta_j - \theta_1), \quad (18)$$

$$\dot{\theta}_j = \omega_j, \quad (19)$$

for $j = 2, 3, \dots, N_c$, where N_c is the number of oscillators on the same ring, and θ_1 is the phase of the oscillator about to be phase-locked. Introducing the phase difference $\Delta\theta_j = \theta_j - \theta_1$ and $\Delta\omega_j = \omega_j - \omega_1$, we have:

$$\Delta\dot{\theta}_j = \Delta\omega_j + \lambda \sum_{k=2}^{N_c} A_{jk} \sin \Delta\theta_k. \quad (20)$$

Each oscillator only needs to be phase-locked with neighboring oscillators (minimum $|\Delta\omega_j|$) to achieve phase locking of entire ring due to the symmetry. The minimum $|\Delta\omega_j|$ in a ring is $|\Delta\omega_j| = (\omega_{\max} - \omega_{\min})/N_c$. When $\lambda \sum_{k=2}^{N_c} A_{jk} \geq |\Delta\omega_j|$, Eq. (20) has fixed point solutions, and the oscillators are phase-locked. Therefore, the critical coupling strength λ_{c1} is:

$$\lambda_{c1} = \frac{\omega_{\max} - \omega_{\min}}{N_c \sum_{j=2}^{N_c} A_{1j}}, \quad (21)$$

where $\sum_{j=2}^{N_c} A_{1j}$ is the number of oscillators within the action scope of the 1st oscillator on the ring. Obviously, this is a function of d_0 . We define it as

$$N_1(d_0) = N_c \frac{S_1(d_0)}{S_R} = \frac{N_c S_1(d_0)}{\pi(r_{\max}^2 - r_{\min}^2)}, \quad (22)$$

where S_1 is the overlapping area of the action scope of the 1st oscillator and the ring, S_R is the area of the ring, and $r_{\max} = v/\omega_{\min}$ and $r_{\min} = v/\omega_{\max}$ are the outer and inner radius of the ring, respectively. In order to achieve phase locking of all oscillators on the ring, we need to consider the minimum value of $N_1(d_0)$. As shown in Fig. 9a, the 1st oscillator is at point A which is on the outer edge of the ring, and the overlapping area of the yellow circle (action scope) and the red ring is $S_1(d_0)$. Elementary geometry gives

$$\begin{cases} S_1(d_0) = d_0^2 \frac{\alpha}{2} + r_{\max}^2 \frac{\beta}{2} - r_{\max} d_0 \sin \frac{\alpha}{2} \\ \beta = 2\arccos\left(1 - \frac{d_0^2}{2r_{\max}^2}\right) \\ \alpha = \pi - \frac{\beta}{2} \end{cases}, \quad (23)$$

where α and β are the angles of sectors from two overlapping circles' centers. Overall, we have

$$\begin{cases} \lambda_{c1} = \frac{\pi(r_{\max}^2 - r_{\min}^2)(\omega_{\max} - \omega_{\min})}{N_c^2 \left(d_0^2 \frac{\alpha}{2} + r_{\max}^2 \frac{\beta}{2} - r_{\max} d_0 \sin \frac{\alpha}{2} \right)} \\ \beta = 2\arccos\left(1 - \frac{d_0^2}{2r_{\max}^2}\right) \\ \alpha = \pi - \frac{\beta}{2} \end{cases}. \quad (24)$$

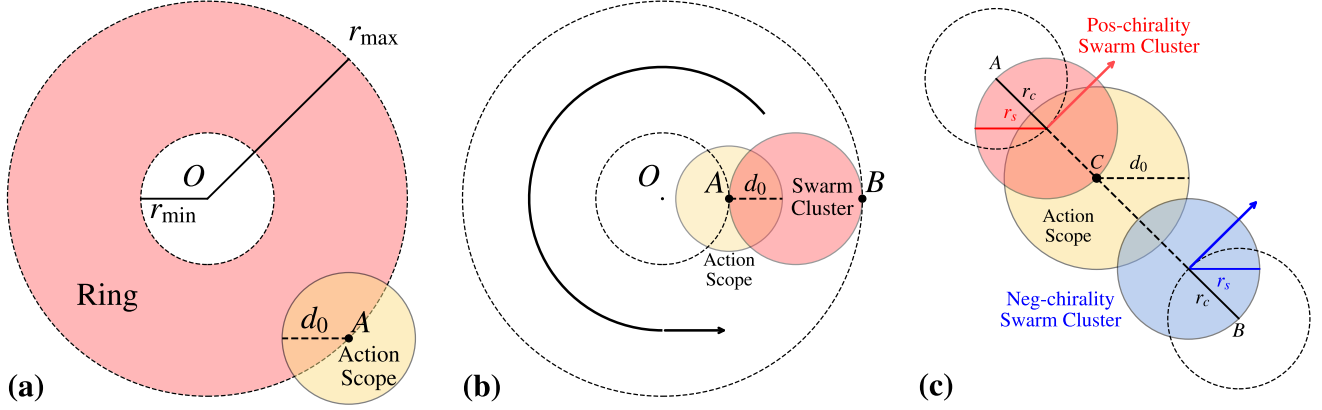


FIG. 9. The schematic plot of the analytical approximations. (a), The 1st oscillator is at point A which is on the outer edge of the ring, and the overlapping area of the yellow circle (action scope) and the red ring is $S_1(d_0)$. (b), The 1st oscillator is at point A which is on the inner edge of the ring, and the overlapping area of the yellow circle (action scope) and the red ring is $S_2(d_0)$. (c), The 1st oscillator is at point C which is on the edge of red circle, and the overlapping area of the yellow circle (action scope) and the blue circle is $S_3(d_0)$.

Then we can calculate the critical line λ_{c1} in the $(\lambda-d_0)$ plane with $N_c = 250$ (Ring state first appears as four rings, more details in Subsection V C), as shown in Fig. 7c, where the line accurately divides the phase-locked and non-phase-locked regions.

2. λ_{c2} : Ring to Swarm (Multi-Clusters)

According to R_s in Fig. 7b, the oscillators in the cluster are synchronized, and the oscillators with different chirality are not synchronized. Therefore, λ_{c2} is the critical value of λ for the synchronization of oscillators in the same cluster. We still consider the synchronous dynamics in Eq. (18) and (19). To achieve synchronization, the oscillators with the largest phase difference (maximum $|\Delta\omega_j|$) in the cluster need to be phase locked. The maximum $|\Delta\omega_j|$ in a cluster is $|\Delta\omega_j| = \omega_{\max} - \omega_{\min}$. Thus, the critical coupling strength λ_{c2} is:

$$\lambda_{c2} = \frac{\omega_{\max} - \omega_{\min}}{\sum_{j=2}^{N_s} A_{1j}}, \quad (25)$$

where N_s is the number of oscillators in the cluster, and $\sum_{j=2}^{N_s} A_{1j}$ is the number of oscillators within the action scope of the 1st oscillator in the cluster, which is $N_2(d_0)$. We define it as

$$N_2(d_0) = N_s \frac{S_2(d_0)}{S_S} = \frac{N_s S_2(d_0)}{\pi r_s^2}, \quad (26)$$

where S_2 is the overlapping area of the action scope of the 1st oscillator and the cluster, S_S is the area of the cluster. Considering that this is a phase transition between ring and cluster states, the oscillator moves with a rotational radius in the ring state until it gathers into clusters, so the radius of the cluster r_s is $(r_{\max} - r_{\min})/2$, as shown in Fig. 9b. Similar to Eq. (23), the

minimum overlapping area S_2 (overlapping area of two circles in Fig. 9b) can be calculated as

$$\begin{cases} S_2(d_0) = d_0^2 \frac{\alpha}{2} + r_s^2 \frac{\beta}{2} - r_s d_0 \sin \frac{\alpha}{2} \\ \beta = 2 \arccos \left(1 - \frac{d_0^2}{2r_s^2} \right) \\ \alpha = \pi - \frac{\beta}{2} \end{cases}. \quad (27)$$

Therefore, we have

$$\begin{cases} \lambda_{c2} = \frac{\pi r_s^2 (\omega_{\max} - \omega_{\min})}{N_s (d_0^2 \frac{\alpha}{2} + r_s^2 \frac{\beta}{2} - r_s d_0 \sin \frac{\alpha}{2})} \\ \beta = 2 \arccos \left(1 - \frac{d_0^2}{2r_s^2} \right) \\ \alpha = \pi - \frac{\beta}{2} \\ r_s = \frac{r_{\max} - r_{\min}}{2} \end{cases}. \quad (28)$$

Then we can calculate the critical line λ_{c2} in the $(\lambda-d_0)$ plane with $N_s = 500$ (each chirality has half of the total population $N = 1000$), as shown in Fig. 7b, where the line divides whether local synchronization occurred.

3. λ_{c3} : Multi-Clusters to Double-Clusters

The derivation of λ_{c3} is similar to that of λ_{c2} , but the difference is that the centers of oscillators in the Swarm (Double-Clusters) state converge quickly (cf Fig. 6b), which means oscillators do not require a long transient to form clusters. We consider that the oscillator density ρ (Number of oscillators per unit area) under initial conditions can achieve synchronization of oscillators of the same chirality. ρ can be calculated as

$$\rho = \frac{N}{L^2}. \quad (29)$$

Then we have

$$\sum_{j=2}^{N_c} A_{1j} = \rho \pi d_0^2 = \frac{N\pi d_0^2}{L^2}. \quad (30)$$

The critical coupling strength λ_{c3} is:

$$\lambda_{c3} = \frac{L^2(\omega_{\max} - \omega_{\min})}{N\pi d_0^2}. \quad (31)$$

Similarly, we can calculate the critical line λ_{c3} in the $(\lambda\text{-}d_0)$ plane, as shown in Fig. 7b, where the values of region above the line (Double-Clusters) is closer to 1 than below the line (Multi-Clusters).

4. λ_{c4} : Swarm (Double-Clusters) to Quick Sync

The Quick Sync state can be considered as a special case of the Swarm state where the oscillators are globally synchronized. Our derivation approach comes from adiabatic parameter tuning (see Appendix D). We assume that the oscillators of two chiralities have been synchronized in the Swarm (Double-Clusters) state, as is shown in Fig. 9c. Next, we consider the synchronization of the two chiralities. According to Eq. (13), two clusters with opposite chirality are moving on their respective circular trajectories with the same rotational radius

$$r_c = \frac{2v}{\omega_{\max} + \omega_{\min}}. \quad (32)$$

In numerical simulations, we observe that the radius r_s of clusters in Swarm state increases with the increase of λ and d_0 . Thus, the radius of the clusters reach maximum value of r_c (see proof in Appendix E) when the λ and d_0 reach the critical values.

Considering that the trajectories of two chiralities will repel each other before oscillators achieving global synchronization, let's take the maximum relative distance between the motion trajectories of two clusters in space, which is line AB in Fig. 9c. The distance l_{AB} is

$$l_{AB} = \frac{L}{\sqrt{2}}. \quad (33)$$

Similar to the derivation of λ_{c2} , we consider the synchronization dynamics between a single oscillator (C in Fig. 9c) and a cluster (blue circle in Fig. 9c), the difference is that the single oscillator and cluster here belong to different chirality. When the centers of two clusters move onto line segment AB , their distance is the shortest. At this point, due to symmetry, if the oscillators at the edges of the two clusters are synchronized, global synchronization can be achieved. Obviously, when

$$d_0 + 2r_c + 2r_s < l_{AB}, \quad (34)$$

the action scope of oscillator at point C does not overlap with the neg-chirality cluster (blue circle), so the critical coupling

strength λ_{c4} does not exist. When $d_0 + 2r_c + 2r_s > l_{AB}$, the overlapping area $S_3(d_0)$ can be calculated as

$$\begin{cases} S_3(d_0) = r_s^2 \frac{\alpha}{2} + d_0^2 \frac{\beta}{2} - d_0 r_d \sin \frac{\beta}{2} \\ r_d = \frac{L}{\sqrt{2}} - r_s - 2r_c \\ \beta = 2\arccos \frac{d_0^2 + r_d^2 - r_s^2}{2d_0 r_d} \\ \alpha = 2\arccos \frac{r_s^2 + r_d^2 - d_0^2}{2r_s r_d} \end{cases}, \quad (35)$$

where $r_s = r_c$. The global maximum value of $|\Delta\omega_j|$ is $\omega_{\max} - (-\omega_{\max}) = 2\omega_{\max}$. Therefore, we have

$$\begin{cases} \lambda_{c4} = \frac{2\pi r_s^2 \omega_{\max}}{N_c \left(\frac{1}{2} r_s^2 + \frac{1}{2} d_0^2 - d_0 r_d \sin \frac{\beta}{2} \right)} \\ r_d = \frac{L}{\sqrt{2}} - r_s - 2r_c \\ \beta = 2\arccos \frac{d_0^2 + r_d^2 - r_s^2}{2d_0 r_d} \\ \alpha = 2\arccos \frac{r_s^2 + r_d^2 - d_0^2}{2r_s r_d} \end{cases}. \quad (36)$$

Then we can calculate the critical line λ_{c4} in the $(\lambda\text{-}d_0)$ plane, as shown in Fig. 7a, where the line divides whether global synchronization occurred.

B. Repulsion-attraction mechanism from chiralities

In the Ring state, the oscillators of two chiralities exhibit a spatial repulsion-attraction mechanism driven by phase coupling. Specifically, the motion trajectories of chiral oscillators of the same chirality are attracted to each other, while the motion trajectories of chiral oscillators of different chirality repel each other. Considering that the ring state occurs when the coupling strength λ and the action radius d_0 are small and the trajectories of the oscillators in the Ring state are almost circular under uncoupled conditions, we can analyze the repulsion-attraction mechanism by considering the motion trajectories of the oscillators.

Under the assumption of no coupling, the center \mathbf{c}_i of the i th oscillator moves on a circular trajectory with radius $r_i = v/\omega_i$ and angular velocity ω_i according to Eq. (8). The coordinates of the rotation center can be estimated as the mean coordinates of points on the trajectory. the horizontal ordinate of the i th oscillator's rotation center is

$$\begin{aligned} C_{xi}(t_0) &= \frac{\omega_i}{2\pi} \int_{t_0}^{t_0+2\pi/\omega_i} \left\{ x_i^0(t_0) + \frac{v}{\omega_i} \sin [\theta_i(t_0) + \omega_i t] \right\} dt \\ &= x_i^0(t_0) \\ &= x_i(t_0) - \frac{v}{\omega_i} \sin \theta_i(t_0). \end{aligned} \quad (37)$$

Similarly, the vertical ordinate of the i th oscillator's rotation center is

$$C_{yi}(t_0) = y_i(t_0) + \frac{v}{\omega_i} \cos \theta_i(t_0). \quad (38)$$

Due to the symmetry of the ring, we can consider the interaction between only two oscillators. For the i th and j th oscillators, the distance between their rotation centers $|\mathbf{c}_j - \mathbf{c}_i|$

is

$$|\mathbf{c}_j - \mathbf{c}_i| = \sqrt{\left(x_j - \frac{v}{\omega_j} \sin \theta_j - x_i + \frac{v}{\omega_i} \sin \theta_i \right)^2 + \left(y_j + \frac{v}{\omega_j} \cos \theta_j - y_i - \frac{v}{\omega_i} \cos \theta_i \right)^2}. \quad (39)$$

Considering the action radius d_0 is small, the coordinates of the two oscillators are very close to each other when coupling occurs, which means $(x_i, y_i) \approx (x_j, y_j)$. Then we have

$$|\mathbf{c}_j - \mathbf{c}_i| = \sqrt{-\frac{2v^2 \cos(\theta_i - \theta_j)}{\omega_i \omega_j} + \frac{v^2}{\omega_i^2} + \frac{v^2}{\omega_j^2}}. \quad (40)$$

Furthermore, due to the symmetry of coupling from Eq. (3), The phase of the two oscillators after being coupled will have a pair of symmetrical angular offsets compared to those without coupling:

$$\begin{aligned} \hat{\theta}_i &= \theta_i + \lambda \sin(\theta_j - \theta_i) T, \\ \hat{\theta}_j &= \theta_j + \lambda \sin(\theta_i - \theta_j) T. \end{aligned} \quad (41)$$

Let's set $\theta_s = \lambda \sin(\theta_j - \theta_i) T$ as the angular offset and θ_s clearly satisfies

$$\theta_s \in \begin{cases} \left[0, \frac{\theta_i - \theta_j}{2}\right], & \theta_j \geq \theta_i \\ \left[\frac{\theta_i - \theta_j}{2}, 0\right), & \theta_j < \theta_i \end{cases} \quad (42)$$

Then we have the distance driven by the coupling $|\hat{\mathbf{c}}_j - \hat{\mathbf{c}}_i|$ as

$$\begin{aligned} |\hat{\mathbf{c}}_j - \hat{\mathbf{c}}_i| &= \sqrt{-\frac{2v^2 \cos(\hat{\theta}_i - \hat{\theta}_j)}{\omega_i \omega_j} + \frac{v^2}{\omega_i^2} + \frac{v^2}{\omega_j^2}} \\ &= \sqrt{-\frac{2v^2 \cos(\theta_i - \theta_j + 2\theta_s)}{\omega_i \omega_j} + \frac{v^2}{\omega_i^2} + \frac{v^2}{\omega_j^2}}. \end{aligned} \quad (43)$$

To compare Eq. (39) and Eq. (43), we only need to compare the cosine term in the two equations. According to Inequality (42), we have

$$\theta_i - \theta_j + 2\theta_s \in \begin{cases} [0, \theta_i - \theta_j], & \theta_i - \theta_j \geq 0 \\ [\theta_i - \theta_j, 0), & \theta_i - \theta_j < 0 \end{cases}, \quad (44)$$

which means

$$\cos(\theta_i - \theta_j) \leq \cos(\theta_i - \theta_j + 2\theta_s). \quad (45)$$

Therefore, when the coupling occurs, the distance between the rotation centers of two oscillators with the same signs of natural frequency ω (chirality) will decrease, which means the oscillators of the same chirality are attracted to each other, while the distance between the centers with opposite signs of ω (chirality) will increase, which means the oscillators of different chirality repel each other.

C. Number of Rings

VI. CONCLUSIONS

Appendix A: PROOF OF THE ADJUSTED POSITION

In this section, we prove the distances between oscillators' adjusted position is the minimum distance in periodic boundary conditions.

Proof. To prove this, we only need to prove the adjusted distance $|\mathbf{r}_i - \bar{\mathbf{r}}_j|$ is not longer than the raw distance $|\mathbf{r}_i - \mathbf{r}_j|$.

For $(x_i - x_j)^2$ and $(x_i - \bar{x}_j)^2$, if $x_j = \bar{x}_j$, we have $(x_i - x_j)^2 = (x_i - \bar{x}_j)^2$. If $x_j \neq \bar{x}_j$, we have

$$\begin{aligned} (x_i - \bar{x}_j)^2 - (x_i - x_j)^2 &= (x_j \pm L - x_i)^2 - (x_j - x_i)^2 \\ &= \begin{cases} L^2 + 2L(x_j - x_i), & x_i - x_j > L/2 \\ L^2 - 2L(x_j - x_i), & x_i - x_j < L/2 \end{cases} \\ &< L^2 - L^2 \\ &= 0 \end{aligned} \quad (A1)$$

Then, we have $(x_i - \bar{x}_j)^2 \leq (x_i - x_j)^2$. Similarly, we have $(y_i - \bar{y}_j)^2 \leq (y_i - y_j)^2$. Therefore, we have

$$\begin{aligned} |\mathbf{r}_i - \bar{\mathbf{r}}_j| &= \sqrt{(x_i - \bar{x}_j)^2 + (y_i - \bar{y}_j)^2} \\ &\leq \sqrt{(x_i - x_j)^2 + (y_i - y_j)^2} \\ &= |\mathbf{r}_i - \mathbf{r}_j|. \end{aligned} \quad (A2)$$

□

Appendix B: NUMERICAL METHODS

All the simulations of the model Eq. (1)-(3) were run on Python using Euler integration, with a time step $\Delta t = 0.01$, and a total time of $T = 60000$.

Appendix C: DETERMINATION OF DBSCAN'S PARAMETERS

DBSCAN (Density-Based Spatial Clustering of Applications with Noise) is a density-based clustering algorithm, which can find clusters of arbitrary shapes and sizes. The algorithm has two parameters: ϵ and m . ϵ is the maximum distance between two samples for one to be considered as in the neighborhood of the other, and m is the minimum number of samples in a neighborhood for a point to be considered as a core point.

We traverse all values between 0.15 and 0.5 with a step length of 0.05, and for each value of ϵ , we calculate the number of clusters of Swarm state with $m = 5$ (which is 0.5% of

the population $N = 1000$ of the system). Then we record the minimum counts of clusters in total states.

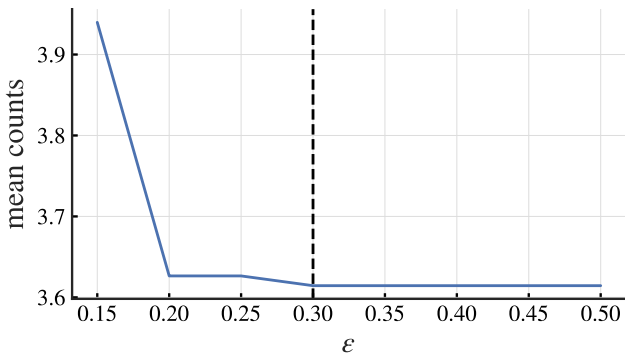


FIG. 10. The minimum counts of clusters with $m = 0$ and different ϵ . The number of clusters is calculated by DBSCAN algorithm.

As shown in Fig. 10, the mean counts of clusters converges to at $\epsilon = 0.3$. Then we set ϵ to be 0.3, and set m to be 5.

Appendix D: ADIABATIC TUNING OF THE ACTION RADIUS

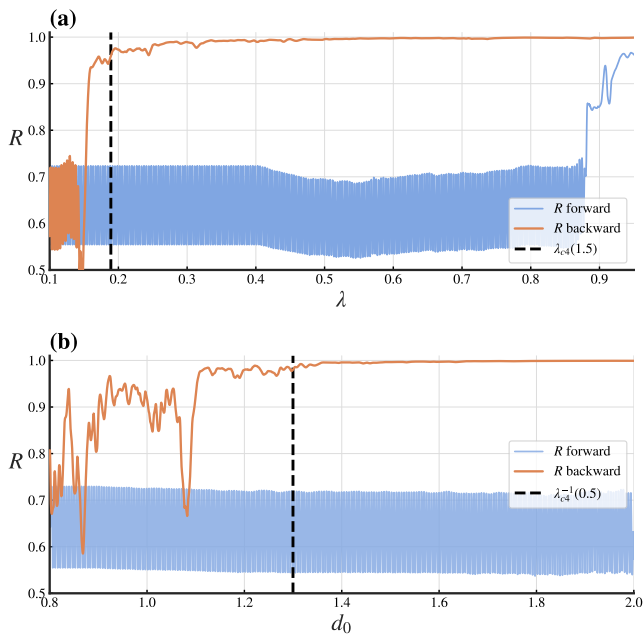


FIG. 11. The adiabatic tuning of the coupling strength λ and the action radius d_0 . (a), The coupling strength λ is adiabatically tuned from 0.01 to 0.95 with fixed $d_0 = 1.5$. (b), The action radius d_0 is adiabatically tuned from 0.8 to 2 with fixed $\lambda = 0.5$.

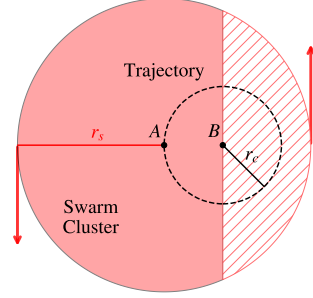


FIG. 12. The schematic plot of the proof of the maximum radius of clusters.

Appendix E: PROOF OF THE MAXIMUM RADIUS OF CLUSTERS

In this section, we prove the maximum radius of cluster in the Swarm state is r_c , which is the radius of its rotation trajectory. We prove this by contradiction.

Proof. We assume that the maximum radius of the cluster is $r_s > r_c$. Then we have the case that the cluster's rotation center is inside the cluster circle with radius r_s . Fig. 12 shows the schematic plot of this case. A and B is the center of the cluster and trajectory circle, respectively. The cluster circle is divided into two parts by B : red solid and red // hatching. In order to enable clusters to move along trajectories, the oscillators in two parts must have contrary phase velocities. This contradicts the fact that the oscillators in the cluster are synchronized. Therefore, the maximum radius of the cluster is r_c . \square

¹A. Pikovsky, M. Rosenblum, and J. Kurths, *Synchronization, A Universal Concept in Nonlinear Sciences*, Vol. 2 (Cambridge University Press, 2001) p. 3.

²J. A. Acebrón, L. L. Bonilla, C. J. P. Vicente, F. Ritort, and R. Spigler, “The kuramoto model: A simple paradigm for synchronization phenomena,” *Reviews of modern physics* **77**, 137 (2005).

³F. A. Rodrigues, T. K. D. Peron, P. Ji, and J. Kurths, “The kuramoto model in complex networks,” *Physics Reports* **610**, 1–98 (2016).

⁴S. Boccaletti, A. N. Pisarchik, C. I. Del Genio, and A. Amann, *Synchronization: from coupled systems to complex networks* (Cambridge University Press, 2018).

⁵W. Zou, D. Senthilkumar, M. Zhan, and J. Kurths, “Quenching, aging, and reviving in coupled dynamical networks,” *Physics Reports* **931**, 1–72 (2021).

⁶A. Arenas, A. Díaz-Guilera, J. Kurths, Y. Moreno, and C. Zhou, “Synchronization in complex networks,” *Physics reports* **469**, 93–153 (2008).

⁷L. M. Pecora and T. L. Carroll, “Master stability functions for synchronized coupled systems,” *Physical review letters* **80**, 2109 (1998).

⁸Y. Kuramoto and Y. Kuramoto, *Chemical turbulence* (Springer, 1984).

⁹S. Watanabe and S. H. Strogatz, “Constants of motion for superconducting josephson arrays,” *Physica D: Nonlinear Phenomena* **74**, 197–253 (1994).

¹⁰S. Strogatz, C. Marcus, R. Westervelt, and R. Mirollo, “Simple model of collective transport with phase slippage,” *Physical review letters* **61**, 2380 (1988).

¹¹E. Ott and T. M. Antonsen, “Long time evolution of phase oscillator systems,” *Chaos: An interdisciplinary journal of nonlinear science* **19** (2009).

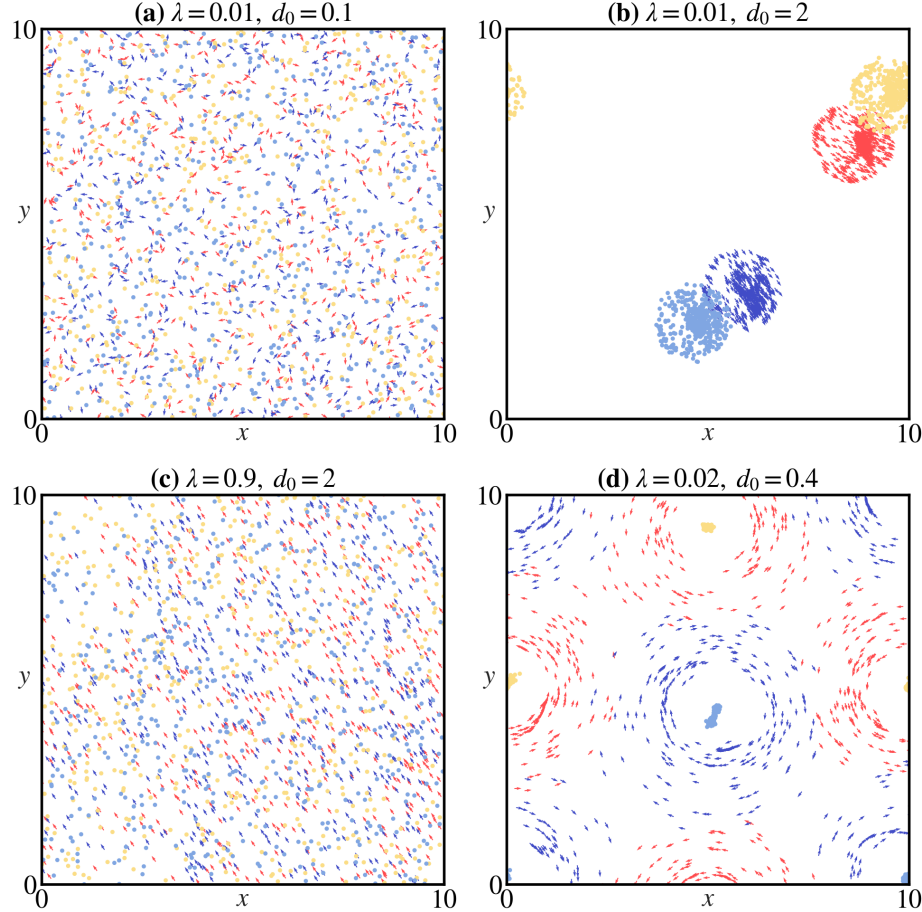


FIG. 13. Estimation results of real-time rotational centers. The centers of two types of chirality oscillators are represented by light yellow ($\omega_i > 0$) and light blue ($\omega_i < 0$) points, respectively. (a), Disorder state ($\lambda = 0.01$, $d_0 = 0.1$). (b), Swarm state, ($\lambda = 0.01$, $d_0 = 2$). (c), Quick Sync stat ($\lambda = 0.9$, $d_0 = 2$). (d), Ring state ($\lambda = 0.02$, $d_0 = 0.4$).

- ¹²J. Buhl, D. J. Sumpter, I. D. Couzin, J. J. Hale, E. Despland, E. R. Miller, and S. J. Simpson, “From disorder to order in marching locusts,” *Science* **312**, 1402–1406 (2006).
- ¹³J. E. Niven, “How honeybees break a decision-making deadlock,” *Science* **335**, 43–44 (2012).
- ¹⁴H. Wioland, E. Lushi, and R. E. Goldstein, “Directed collective motion of bacteria under channel confinement,” *New Journal of Physics* **18**, 075002 (2016).
- ¹⁵E. Lushi, H. Wioland, and R. E. Goldstein, “Fluid flows created by swimming bacteria drive self-organization in confined suspensions,” *Proceedings of the National Academy of Sciences* **111**, 9733–9738 (2014).
- ¹⁶H.-P. Zhang, A. Beer, E.-L. Florin, and H. L. Swinney, “Collective motion and density fluctuations in bacterial colonies,” *Proceedings of the National Academy of Sciences* **107**, 13626–13630 (2010).
- ¹⁷X.-q. Shi and Y.-q. Ma, “Understanding phase behavior of plant cell cortex microtubule organization,” *Proceedings of the National Academy of Sciences* **107**, 11709–11714 (2010).
- ¹⁸D. Debnath, P. K. Ghosh, Y. Li, F. Marchesoni, and B. Li, “Communication: Cargo towing by artificial swimmers,” *The Journal of Chemical Physics* **145** (2016).
- ¹⁹T. Vicsek, A. Czirók, E. Ben-Jacob, I. Cohen, and O. Shochet, “Novel type of phase transition in a system of self-driven particles,” *Physical review letters* **75**, 1226 (1995).
- ²⁰F. Farrell, M. Marchetti, D. Marenduzzo, and J. Tailleur, “Pattern formation in self-propelled particles with density-dependent motility,” *Physical review letters* **108**, 248101 (2012).
- ²¹K. H. Nagai, Y. Sumino, R. Montagne, I. S. Aranson, and H. Chaté, “Collective motion of self-propelled particles with memory,” *Physical review letters* **114**, 168001 (2015).
- ²²R. Großmann, P. Romanczuk, M. Bär, and L. Schimansky-Geier, “Vortex arrays and mesoscale turbulence of self-propelled particles,” *Physical review letters* **113**, 258104 (2014).
- ²³O. Chepizhko, E. G. Altmann, and F. Peruani, “Optimal noise maximizes collective motion in heterogeneous media,” *Physical review letters* **110**, 238101 (2013).
- ²⁴Y. Sumino, K. H. Nagai, Y. Shitaka, D. Tanaka, K. Yoshikawa, H. Chaté, and K. Oiwa, “Large-scale vortex lattice emerging from collectively moving microtubules,” *Nature* **483**, 448–452 (2012).
- ²⁵J. Yan, M. Han, J. Zhang, C. Xu, E. Luijten, and S. Granick, “Reconfiguring active particles by electrostatic imbalance,” *Nature materials* **15**, 1095–1099 (2016).
- ²⁶J. Pantaleone, “Stability of incoherence in an isotropic gas of oscillating neutrinos,” *Physical Review D* **58**, 073002 (1998).
- ²⁷K. Wiesenfeld, P. Colet, and S. H. Strogatz, “Synchronization transitions in a disordered josephson series array,” *Physical review letters* **76**, 404 (1996).
- ²⁸I. Aihara, H. Kitahata, K. Yoshikawa, and K. Aihara, “Mathematical modeling of frogs calling behavior and its possible application to artificial life and robotics,” *Artificial Life and Robotics* **12**, 29–32 (2008).
- ²⁹K. P. O’Keeffe and S. H. Strogatz, “Dynamics of a population of oscillatory and excitable elements,” *Physical Review E* **93**, 062203 (2016).
- ³⁰Z. Néda, E. Ravasz, T. Vicsek, Y. Brechet, and A.-L. Barabási, “Physics of the rhythmic applause,” *Physical Review E* **61**, 6987 (2000).

- ³¹S. Majhi, D. Ghosh, and J. Kurths, “Emergence of synchronization in multiplex networks of mobile rössler oscillators,” Physical Review E **99**, 012308 (2019).